Hindawi
International Journal of Antennas and Propagation
Volume 2022, Article ID 8940715, 11 pages
https://doi.org/10.1155/2022/8940715

Research Article

5G Millimeter Wave Endfire Array Antenna with Printed Inverted-F Structure

Shang Feng, Xu Xin, and Ren Chuxuan

School of Electronic Engineering, Xi'an University of Post & Telecommunications, Xi'an 710121, China

Correspondence should be addressed to Xu Xin; renchuxuan@stu.xupt.edu.cn

Received 24 May 2022; Revised 25 July 2022; Accepted 27 July 2022; Published 12 August 2022

Academic Editor: Rajkishor Kumar

In this design, a novel inverted F antenna with a low profile feed structure is proposed for millimeter-wave (mmW) applications. The array element consists of a printed inverted F antenna and a L-shaped parasitic deflector, approximately forming a structure similar to the Yagi-Uda antenna. The gain could be increased and the impedance bandwidth could be broadened by the structure. And, it is important to realize the miniaturization of the antenna element by bending the parasitic deflector based on the traditional deflector without affecting the performance. The proposed antenna has a low feed substrate height (0.254 mm~0.02λ_0), which makes it easy to integrate with planar circuits. As proof, a 1×4 array model with an impedance bandwidth of 20.5% (23.0–28.3 GHz) is designed and measured. The inverted F array demonstrated is an important candidate for mmW applications due to its wide bandwidth, miniaturization, ease of integration with planar circuits, and low manufacturing cost.

1. Introduction

As modern communication becomes more and more popular, the number of users increases dramatically. The existing spectrum looks increasingly stretched. Wireless technologies at millimeter-wave (mmW) frequencies have recently received increasing attention due to a large amount of spectrum resources available. For example, 5G communication [1, 2], automotive radar [3, 4], satellite communication [5, 6], synthetic aperture radar [7], broadband high-speed point-pointing communication [8, 9]. It is reported to be in use. And since the transmission loss increases gradually with the frequency during transmission, the millimeter-wave antenna needs to be grouped in an array to improve the gain [10–12]. However, there are also some applications where the user equipment is small, so the antenna is required to be as small as possible to reduce the size of the antenna. To solve this problem, antenna miniaturization has been widely studied in recent years. The miniaturization of the antenna unit is achieved through the topology as shown in the literature [13, 14]. End-emitting radiation antennas in millimeter-wave phased array applications have been studied in the past, such as quasi-Yagi antennas [15, 16], angular dipole antennas, [17, 18] and notch antennas [19].These antennas are suitable for array structures with good performance at various millimeter-wave frequencies. However, most antennas are not suitable for embedding in mobile terminals because of the large horizontal width of the antenna. On the limited area of PCB of the mobile devices, millimeter-wave antennas should be tightly packed with many components used for various functions such as displays, data communications, and cameras. Therefore, it is particularly important to minimize the transverse size of the antenna (including the filling cut area around the antenna) [1]. [20] used a conventional dipoles antenna using the ground plane as a reflector to obtain the end-fire effect, but the gain is relatively small. For the design of the array antenna, the feeding mode is worth a concern. In the traditional feeding mode, a microstrip is used for feeding. For example, a large number of wideband Wilkinson Power divider are used to cover the 8–12 GHz bandwidth; however, the insertion loss of every Wilkinson power divider exceeds 3.5 dB. For example, some end-radiation antennas fed by metal waveguides were studied [21, 22], which showed wider bandwidth and higher radiation efficiency. However, their size and high manufacturing costs may limit their range of applications.

Substrate integrated waveguides(SIW) are integrated with planar circuits or chips because of their high Q value, low insertion loss, low cost, and low profile characteristics. For example, in [23], a low profile is achieved by using a SIW for feeding. [24] applied a hexagonal SIW as a back cavity to design a miniaturized triplexer. SIW can also be used to design back-cavity SIW antennas. Cross-polarization and mutual coupling between the array elements can be effectively reduced [25]. SIWs are also often designed as circularly polarized back-cavity SIW antennas with a high gain due to their cost, and low profile. For example, [26, 27] by etching a square slot in the upper layer of the SIW, and circular polarization is achieved by means of a feed topology. Therefore, for millimeter-wave applications, it is ideal to use SIW to design broadband end-fire array feed networks with low-profile feed structures and low manufacturing costs. In this communication, a novel millimeter-wave end-fire array is proposed and its structure, design process, and measurement results are reported. The array element consists of a horizontal printed inverted F antenna and a bent printed parasitic deflector to obtain a wider impedance bandwidth while compensating for gain. Different from the normal deflector, the bent deflector proposed in this paper can obtain a smaller transverse width while keeping the gain unchanged. This allows the proposed antenna to obtain a smaller array. The low profile SIW feed makes the proposed antenna easy to integrate with the planar front-end circuit. As a demonstration, a 1×4 array was designed and fabricated to validate the proposed design approach. The array has the advantages of broadband, easy integration with planar circuits, low cost, and having a low-profile feed structure. This communication is organized as follows. Section 1 describes the design principles of the proposed antenna elements, and the design of the array is given in Section 2. The corresponding discussion is given in Section 3, and finally, the conclusion is given in Section 4.

2. Design of the Proposed of Inverted F Deflector Antenna Array

The design of the proposed array antenna can be divided into three steps, the designing and optimization of the antenna element, the designing and optimization of the feed network, and the optimization of the cascade of the antenna element with the feed network.

The antenna element is designed using an inverted F antenna as the basic antenna element, and to compensate for its lack of gain, a deflector is added and a bent deflector solution is proposed to miniaturize the antenna element. A suitable antenna element is finally obtained. The design of the feed network takes into account the high operating band and uses the form of a SIW, and due to the small size of the array element spacing and antenna element, a new Y-shaped power divider is proposed. Through cascading, a 1×4 power divider is designed. Then connecting the elements to the cascaded power divider, the whole simulation mode is formed. Finally, the antenna array is produced and measured.

2.1. Design of the Element. Due to their simple construction, inverted F antennas Could be used in user equipment applications. For millimeter waves, there is a problem of high loss in transmission, so the gain needs to be increased to minimize the effect of transmission loss. However, the gain of a traditional printed inverted F antenna is small. In order to compensate for its gain, the current phase and amplitude of the deflector and reflector are controlled by controlling the distance between the deflector, active and reflector using the deflector principle of traditional Yagi antenna. Meanwhile, the length of the deflector and reflector also affects the amplitude and phase of the current. The inductive electromotive force method can be used to analyze the current amplitude and phase relationship between the deflector and the inverted F antenna to verify that the deflector is satisfied. Figure 1(b) shows the inverted F antenna using a conventional deflector. It can be noticed that the length of the conventional deflector is approximately twice as long as the resonator of the inverted F antenna. The conventional deflector, therefore, has a direct impact on the miniaturization of the antenna element. In order to reduce the lateral length of the antenna without affecting the longitudinal length, it is the length of the guide and the distance from the resonator that affect the amplitude and phase of the current between the resonator and the deflector according to the deflecting principle, so the deflector is bent downward while keeping the length of the deflector constant, see Figure 1(a). Figure 2 shows the electric field on the deflector and active antennas of both antennas. It can be seen that there is a strong electric field on the deflector of both, which reflects the fact that both deflectors play a role.

Comparing the two, the lateral length of the deflector is reduced by 26%, but the total length remains unchanged. A comparison of the simulation results is shown in Figure 3(a) and 3(b). Since the gain of the directing antenna is the result of superimposing the energy of the active antenna, the deflector, and the reflector in the X-direction, the bend-directed antenna is the result of superimposing the energy of the antenna. The bending direction is shorter in the Y direction compared to the traditional direction, so the bending direction antenna in the end direction than the traditional direction antenna gain is smaller. When the efficiency of the two antennas is more or less the same, the bandwidth will increase as the gain decreases. Therefore, the bandwidth of the bend-directed antenna is greater than that of the conventional-directed antenna. When the deflector is located directly in front of the active antenna, the Q value of the overall antenna structure is larger than that of the bend-directed antenna, and according to the relationship between bandwidth and quality factor Q. When the Q value decreases, the bandwidth will become larger. So the bandwidth of the bend-directed antenna is slightly wider than that of the conventional deflector. Therefore, the bent deflector reduces the transverse length of the antenna element without much difference from the performance of the traditional deflector. The miniaturization has been achieved.

When the length $L2$ of the bending part is changed, the S-parameters of the antenna element are shown in Figure 4(a) . When the $L1$ of the antenna parasitic deflector is

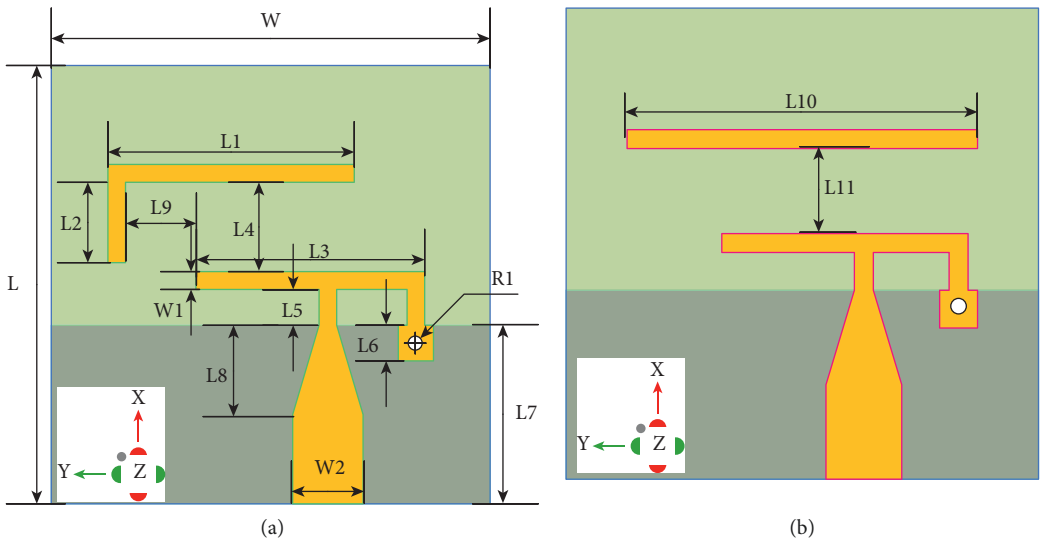

Figure 1: Antenna element structure. (a) Bent parasitic deflector. (b) Traditional parasitic deflector.

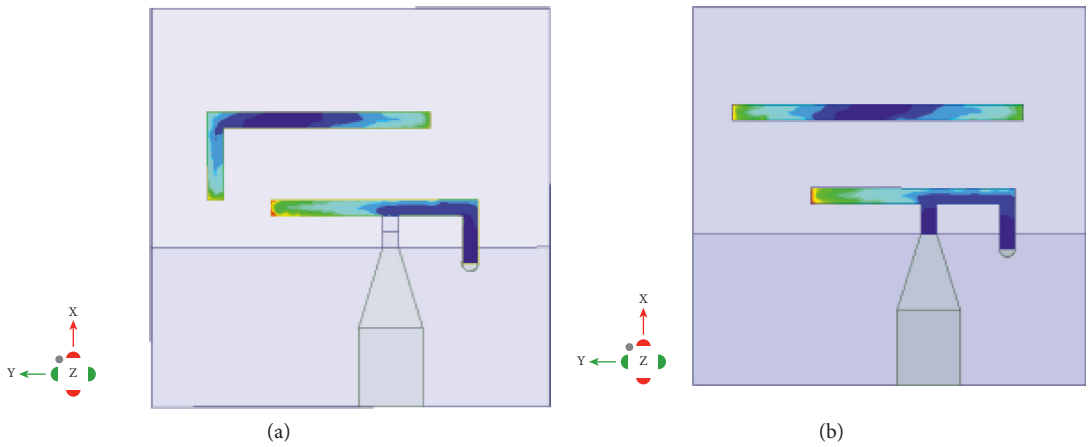

Figure 2: Antenna element electric field diagram. (a) Bent parasitic deflector. (b) Traditional parasitic deflector.

kept constant, the S-parameter gradually moves to high frequency and gradually matches better as $L2$ becomes smaller. Figure 4(b) is the antenna xoy plane direction diagram, it can be seen that with the increase of $L2$, the antenna gain gradually increases. According to the figure, the antenna is slightly left when $L2 = 0.3$ mm, but with the increase of $L2$, the maximum gain point of the antenna arrives in the positive X direction. Meet the lead requirements. According to the results in Figure 4, $L2 = 0.9$ mm was finally selected. At the same time, a better impedance bandwidth and gain are obtained.

For the traditional parasitic deflected antenna, a better guiding effect can be obtained when the deflector is located directly in front of the resonator. However, when the bent deflector is located in front of the antenna, the gain effect is not very good. Therefore, a parametric scan of its lateral distance from the resonator was performed, and it was found that the antenna gain was improved when it was biased to the left of the resonator, and the antenna match in the desired frequency band was gradually satisfied. However, the gain deteriorates as the distance increases. Therefore, the gain is combined with impedance bandwidth, to select an appropriate distance $L9$. The reason is that compared with the traditional oscillator antenna, the main resonator of an inverted F antenna is its long arm, so the deflector device needs to be placed directly in front of it. Therefore, it needs to be offset to the left to meet the requirements. Figure 5(a) and 5(b) is the influence result diagram of different $L9$ on S parameters and gain of antenna element, respectively.

Due to the relatively small electrical size of the antenna, the width $W = 0.2$ mm of the driving element, and the leading element for consideration of processing accuracy, the antenna element needs to be cascaded with the feed network. The cascade method uses the microstrip transition, so the feed transition between the microstrip and the printed array needs to be considered. It can obtain the smooth transition distance $L8$ by software simulation optimization, and then calculate the microstrip line width $W2$. For the short circuit matching part of the antenna part, the metalized through-hole with radius $R1$ is used to realize. So far,

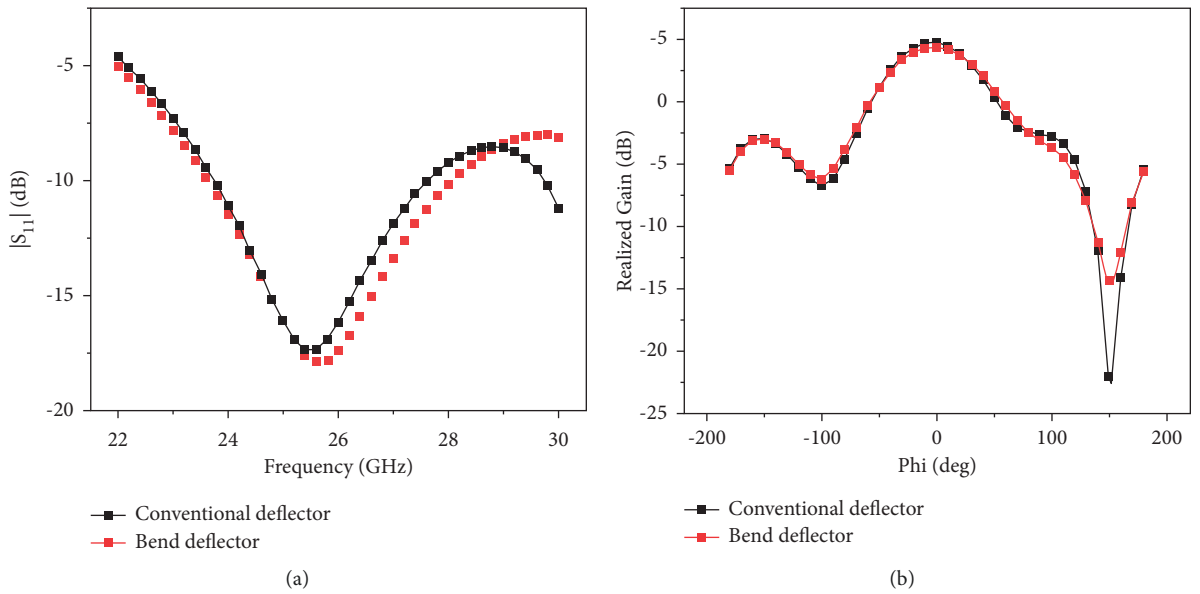

Figure 3: Comparison of simulation results between loaded conventional leading and bent leading antennas. (a) S-parameter comparison. (b) Gain comparison.

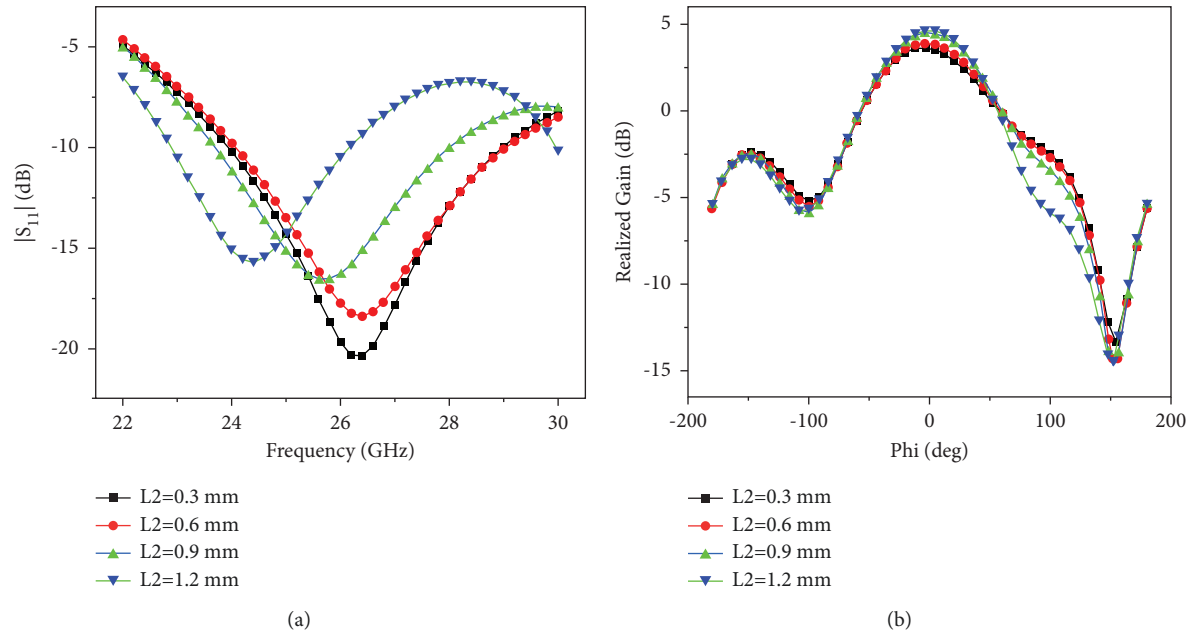

Figure 4: Influence of bender length on the guide. (a) Influence of bender length on $S11$. (b) Influence of different lengths on gain.

the preliminary design of the structure of the antenna element has been completed. The parameters of the antenna structure are shown in Table 1.

The printed circuit board used in this design is Rogers 5880, with a thickness of 0.254 mm and a dielectric constant of $\varepsilon r = 2.2$, loss tangent is 0.0009. The simulation performance of the antenna unit obtained by ANSYS HFSS is shown in the figure. From the simulation results, it can be seen that a single element can achieve 17.3% (23.7–28.2 GHz) impedance width. Figure 6 shows the radiation diagram of the design element, showing the gain performance at 24.75 GHz, 26 GHz, and 27.5 GHz. In general, the proposed element not only realizes end-to-end radiation but also has a thin structure of 0.254 mm, that is, 0.022 λ_0, which can be easily integrated with planar front-end circuits and or chips.

2.2. Antenna Array Design. Considering the large spatial loss in the millimeter-wave band, millimeter-wave generally requires a group array. This design after considering the size and gain choose to do a 1×4 array and considering the

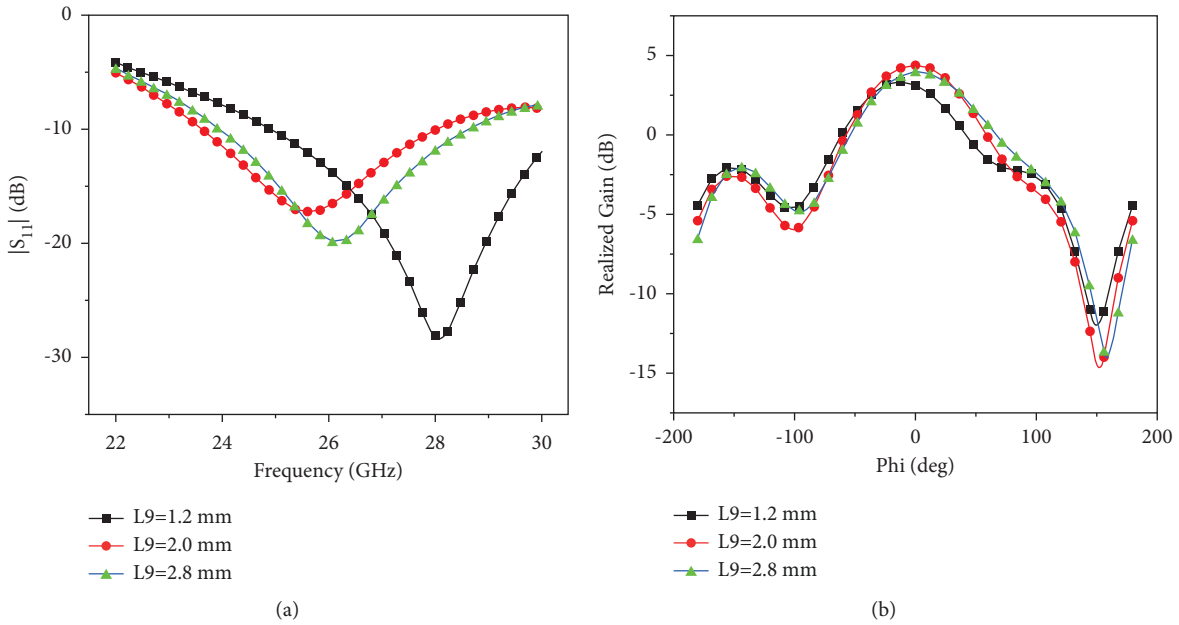

Figure 5: Effect of deflector position on antenna. (a) The influence of different deflector positions on antenna $S11$. (b) The influence of different deflector positions on antenna gain.

Table 1: Antenna unit structure parameter values.

Parameter	Value (mm)	Parameter	Value (mm)
L	5	W	5
$L1$	2.8	$L2$	0.9
$L3$	2.7	$L4$	1
$L5$	0.4	$L6$	0.4
$L7$	2	$L8$	1
$L9$	2	$L10$	3.7
$L11$	1	$W1$	0.2
$W2$	0.8	$R1$	0.1

antenna working band, if it adopted a traditional microstrip line for feeding back, it could lead to excessive insertion loss, energy leakage, and high shielding. SIW has the advantages of low processing cost, low loss, complete shielding, and high-quality factor. Therefore, this paper uses SIW for feeder network design.

The lowest frequency of the desired band should be used as the cutoff frequency when calculating the waveguide width. The feeder network is designed in a cascade manner. The feeder network is designed in a cascade manner. First, the ideal array element spacing $Ld = 7.5$ mm is optimized based on simulation, and then each stage of the feeder network is designed. Since the array is a line array, the power divider in the first and second stage of the cascade needs to bend, there are two-way to turn the way, one is a right-angle turn, and the second is a rounded corner turn. After comparison with right-angle turns, rounded corners can obtain better impedance matching. In rectangular waveguide T-power splitters, the reflection coefficient at the input port is often improved by loading inductive diaphragms or inductive columns. This essay will demonstrate how to achieve the role of the short circuit in a metal column via metalized through-holes. It will make the field in the SIW

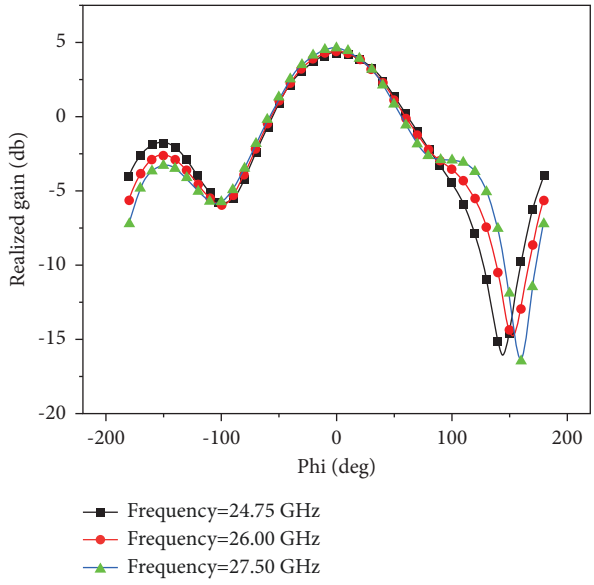

Figure 6: Antenna unit intra-band gain.

form a discontinuity in the H-plane, thus causing the accumulation of magnetic field energy, and therefore has the characteristics of an inductor, often called an inductive column. To obtain a good power distribution, the radius $R2$ and position $L3$ of this shorting column will have a direct impact on the matching of the power divider as well as the insertion loss. Therefore, the design can be adjusted on this basis when it is carried out.

Due to the small size of the millimeter-wave band antennas, the width of the array element spacing is also relatively small, and the larger width of the SIW used will affect the array element spacing, thus affecting the array gain.

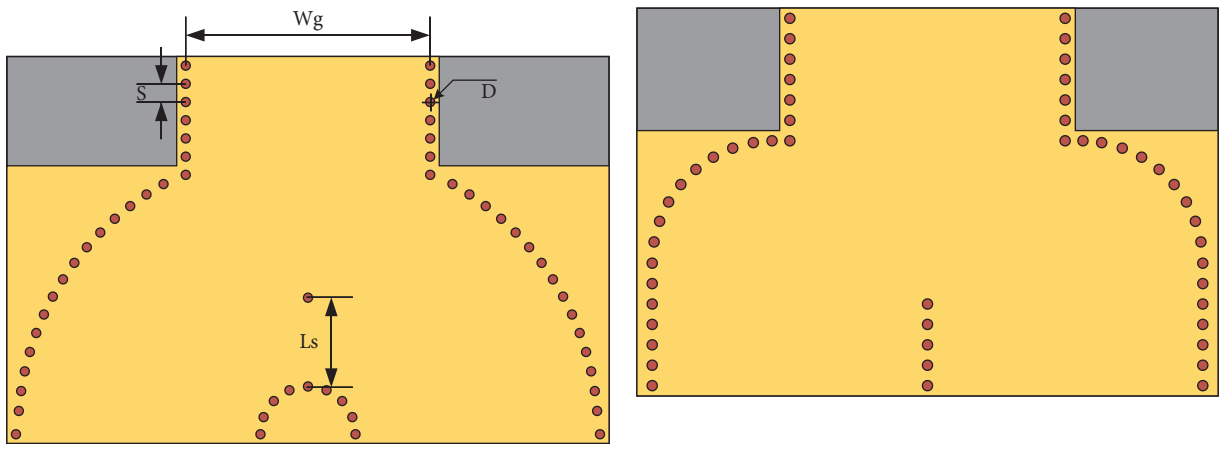

Figure 7: Second stage power divider model: (a) novel; (b) conventional.

Under the condition that the Y-type power divider outputs are close together, if there is an array spacing greater than the length between the two outputs, it is necessary to widen the width of the waveguide to meet the needs of the array spacing. However, this would affect the overall array size. Therefore, a power divider with adjustable array element spacing is designed, and the two outputs are directly rounded and turned. The two rows of metal vias are similar to concentric circles nested together to form a new *Y*-shaped power divider. Figure 7 shows the structural models of two types of power dividers: (a) new *Y*-type power divider, and (b) conventional *Y*-type power divider. *S* is the distance of the through-hole, *D* is the diameter of the through-hole, *Wg* is the width of the waveguide, and *Ls* is the distance of the inductor column position. Figure 8 shows the comparison of the *S*-parameters of the two.

Comparing the two types of power dividers, the impedance matching of the new *Y*-type power divider is better than that of the traditional *Y*-type power divider. And the loss in the frequency band range is also smaller. Based on this, a 1 : 4 power divider with equal amplitude and phase is designed, Figure 9 shows its structure, and its *S*-parameters are shown in Figure 10(a) and 10(b), where the insertion loss is less than 0.6 dB in the desired frequency band 24.75–27.5 GHz, which satisfies the feed network for antenna feeding. Where $D = 0.2$ mm, $Wg = 5.4$ mm, $Ls = 1.9$ mm.

The next step for antenna and feeder network cascade, generally speaking, antenna and feeder network cascade only need direct cascade. However, this antenna has a serious mismatch in the whole matching state of the antenna array after cascading with the feeder network. After analyzing the reason, the use of transition was adopted to cascade the antenna with the feeding network, at this time the array is back to normal. Figure 11 shows the comparison of the antenna *S* parameters and the XOY plane directional diagram of the center frequency point for the two cascade methods. It can be seen that the matching, as well as the gain with the transition structure, is better than the result without the transition structure.

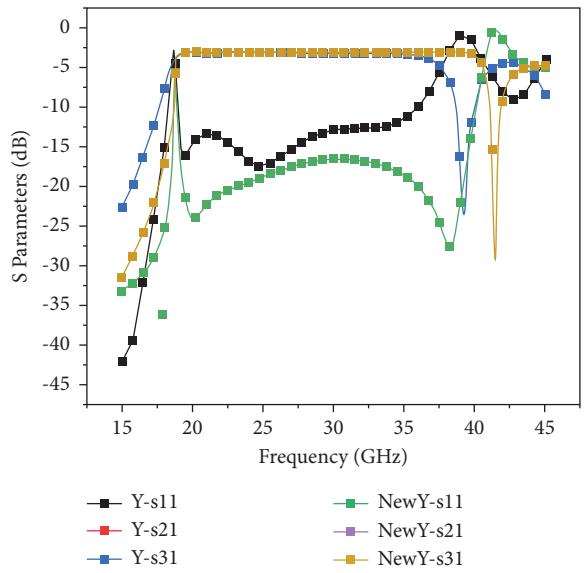

Figure 8: Comparison of S-parameters of new and conventional power dividers.

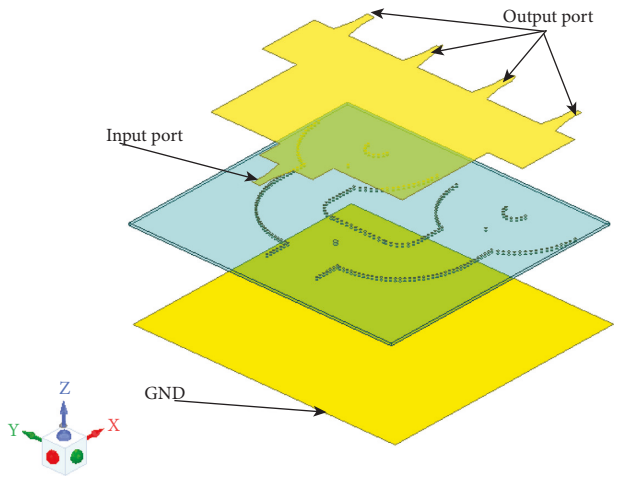

Figure 9: Structural model of a 1 × 4 power divider.

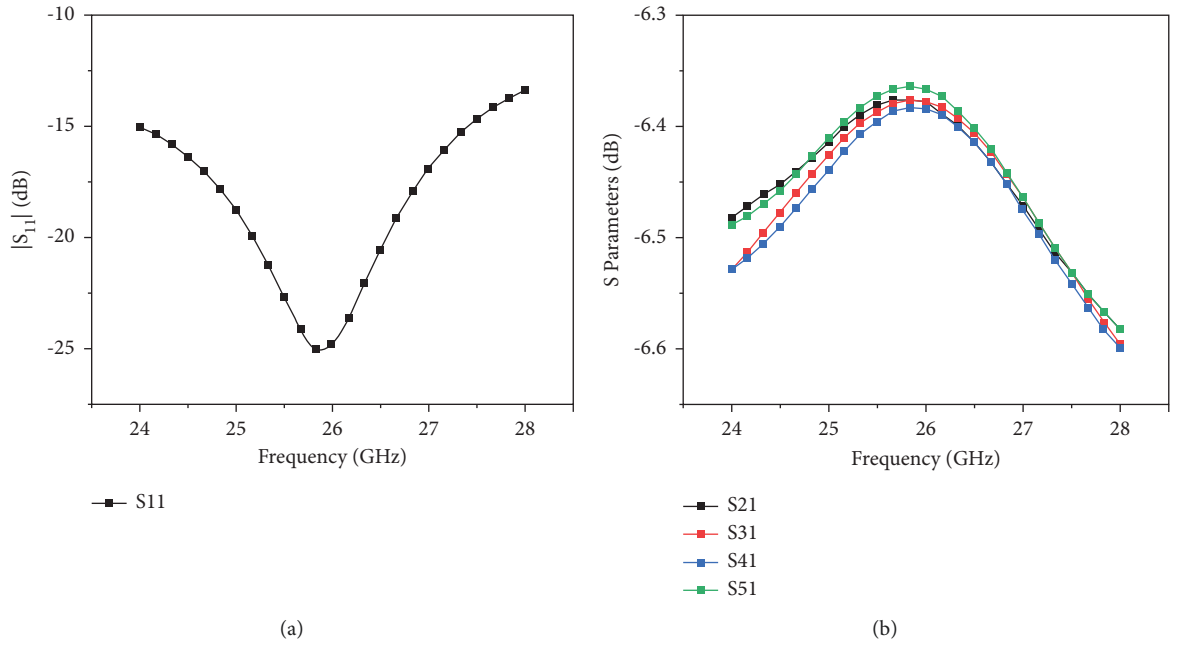

Figure 10: Array feeder network simulation results: (a) input port return loss; (b) individual port insertion loss.

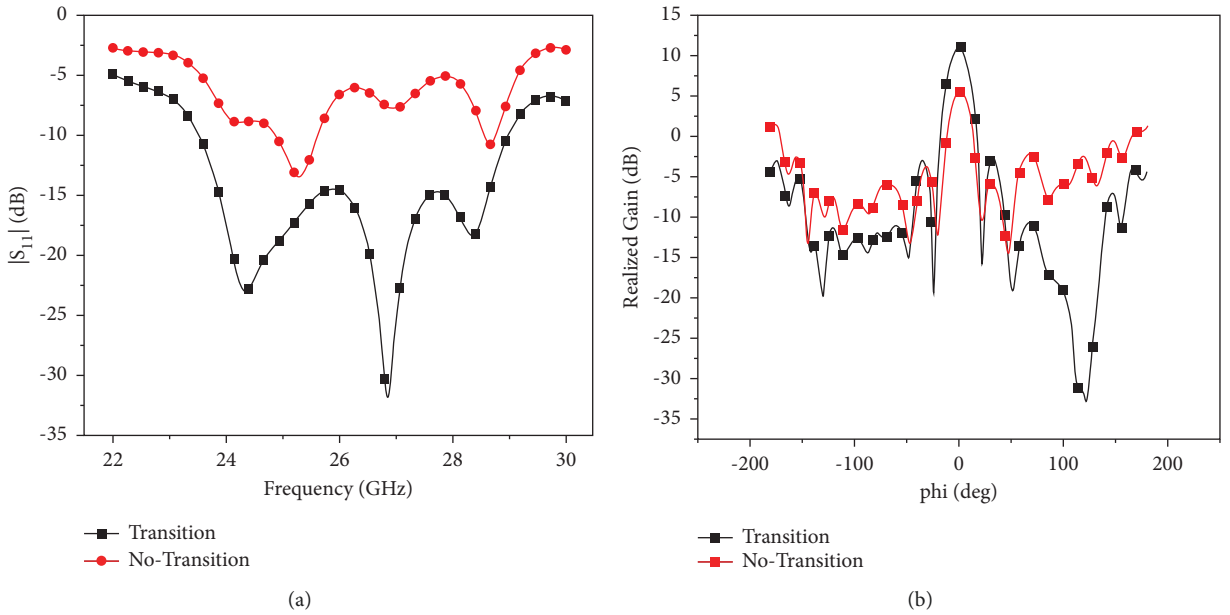

Figure 11: Simulation comparison of different cascade methods: (a) S-parameters; (b) gain.

The structure of the final array is shown in Figure 12 below, the feed network and antenna cascade are in the form of a simple and reliable microstrip line, and the transition between the ground of the antenna element at the grounding layer and the lower metal layer of the feed network is made by a lesser ground compared to the ground of the antenna element, and this metal layer is the ground provided for the upper microstrip line. Among them, by adjusting the transition structure, it is found that different lengths of transition have some influence on the gain of the antenna. An appropriate gain increase is obtained by adjusting its length. And after cascading, the size and position of the short-circuit metallization holes of the feeder network are adjusted to achieve the best performance of the array.

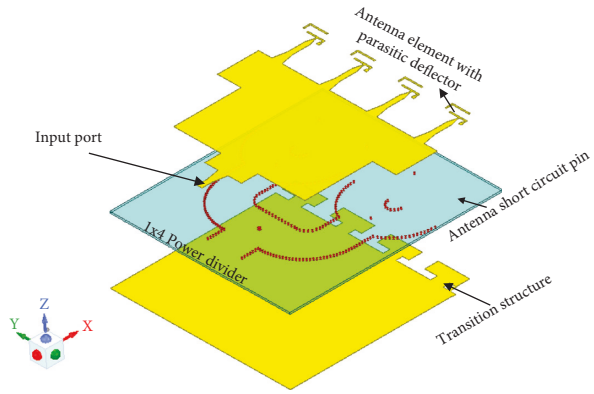

Figure 12: The overall structure of the antenna array.

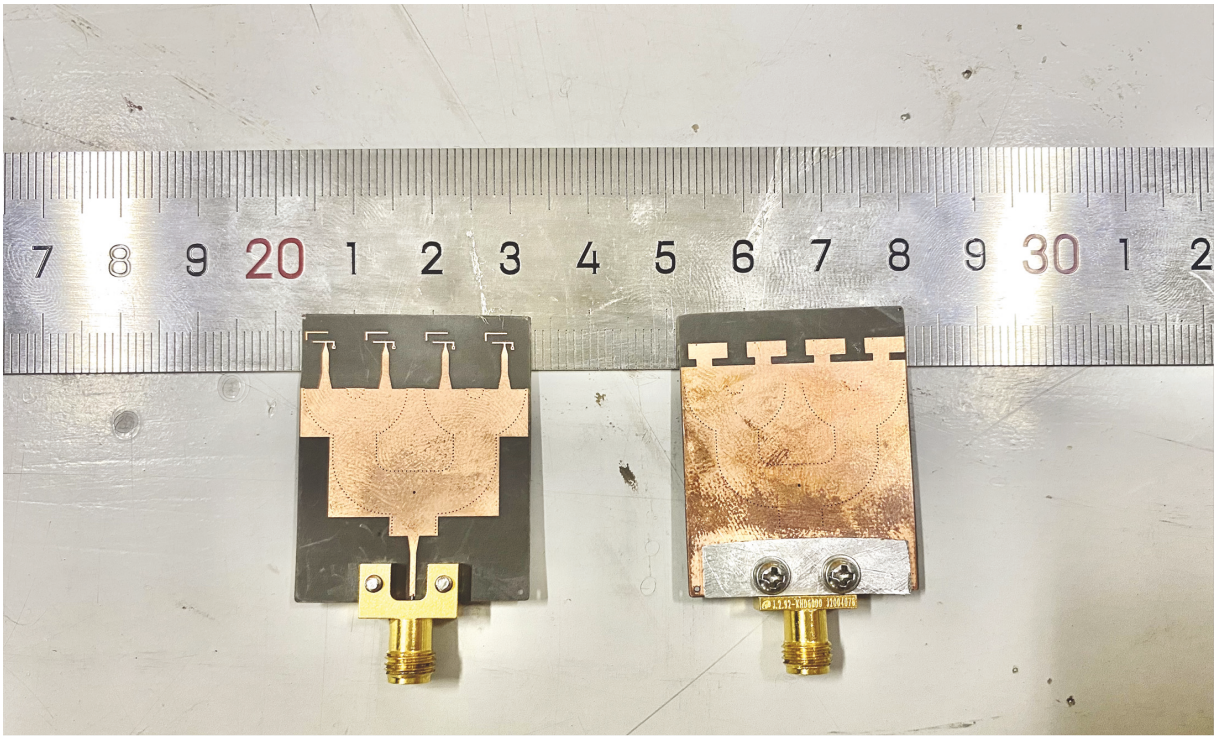

Figure 13: Antenna physical top layer and bottom layer photos.

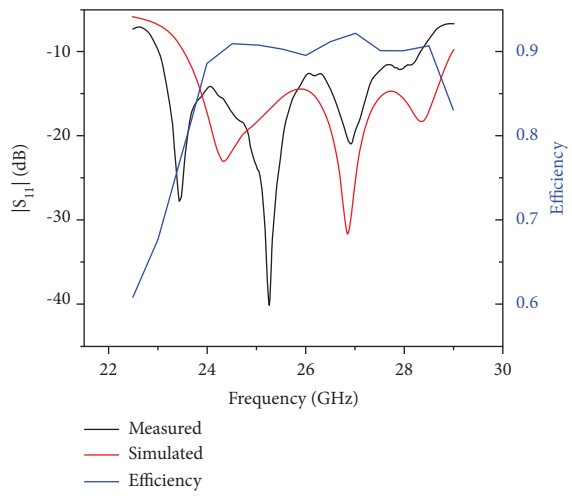

Figure 14: Comparison of measured and simulated S-parameters of antenna array.

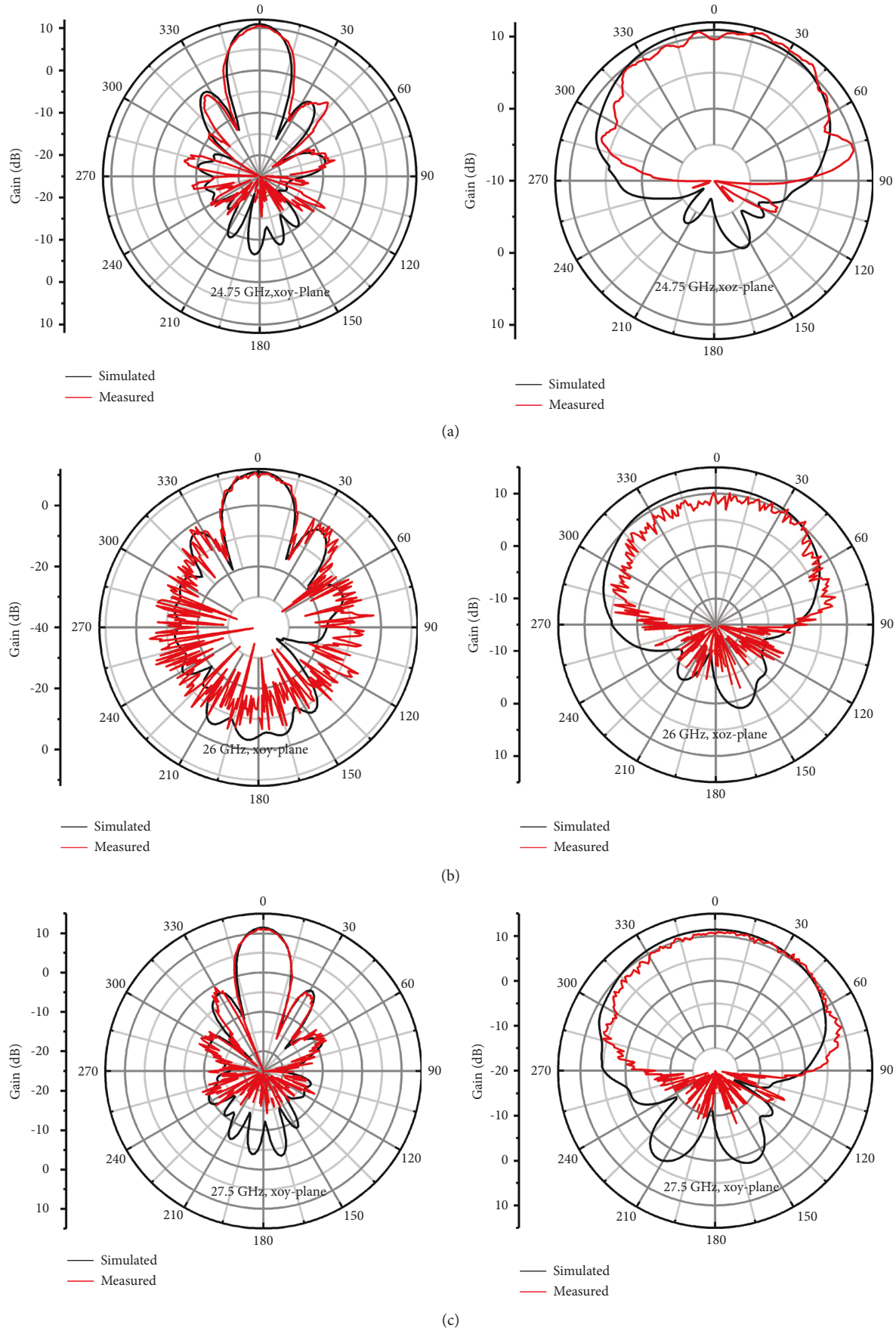

Figure 15: Simulated and measured directional plots of the antenna array at different frequencies. (a) 24.75 GHz. (b) 26 GHz. (c) 27.5 GHz.

Table 2: Performance comparison of other existing millimeter wave end-fire antennas.

Ref.	Antenna element	BW (%)	Relative size (λ_0)	Peak gain (dBi)	Fabric cost
[13]	FoldedDipoled + reflector	26.3–29.75 GHz (12.3%)	$(2.34 \times 2.34 \times 0.068)\lambda_0{}^*$	5.5	High
[14]	FoldedDipoled + reflector	34.0–37.5 GHz (9.7%)	$(2.34 \times 2.34 \times 0.068)\lambda_0$	5.7	Low
[20]	Dipole + reflector	24.9–30.2 GHz (19.2%)	$(0.42 \times 1.74 \times 0.05)\lambda_0$	3.4	Low
This work	IFA	24.08–27.73 GHz (14.1%)	$(0.43 \times 0.43 \times 0.02)\lambda_0$	2.4	Low
This work	IFA + deflector	23.7–28.2 GHz (17.3%)	$(0.43 \times 0.43 \times 0.02)\lambda_0$	4.5	Low

λ_0 is the wavelength at center frequency in free space.

3. Experimental Verification and Discussion

The array was processed based on the structure of the array simulation, and Figure 13 shows the photo of the array, including the top and bottom layers of the array. The $|S11|$ was measured with an Agilent N5432 A vector network analyzer. The simulated and measured $|S11|$ is shown in Figure 14, showing an impedance bandwidth of 20.5% from 23 to 28.3 GHz. The deviation between the simulated and measured results can be observed in Figure 14, where an off-frequency appears, but the waveforms are the same. This may be caused by manufacturing inaccuracies. Figure 14 also shows the simulated efficiency of the array antenna, and it can be seen that the efficiency of the antenna is greater than 0.85 in the frequency band. The radiation direction map, the actual gain of the array was measured in the darkroom. Figure 15 shows the radiation direction plots (xoy plane and xoz plane) for the three frequency points of the array, comparing the simulation results with the measured results. The main radiation direction between the two has a strong consistency, the measured gain is lower than the simulation, and there are many burrs. The analysis may be due to testing errors, inaccurate processing, and increased conductor and dielectric losses at millimeter-wave frequencies. In the actual test, the rear end of the antenna is the antenna mounting table, which had an effect on the rear flap of the antenna. The peak gain measured at 26 GHz and 27.5 GHz reached 11 dB. Therefore, the proposed array not only achieves high gain and miniaturization but also has the advantage of a low-profile feed structure (0.254 mm~0.02 λ_0). However, due to its low-profile feed structure, the proposed array can be easily integrated with planar circuits, which is of practical interest for millimeter-wave systems.

Table 2 compares the performance metrics between the proposed antenna and other existing millimeter-wave end-fire antennas. It can be seen that most of the end-fire antennas listed in Table 2 achieve high gain performance. Considering the antenna miniaturization and low-profile feed structure requirements, the proposed end-fire element has a wider bandwidth as well as small size characteristics compared to the other antennas listed in Table 2. The antennas proposed in [13, 14] both use a folded dipole to obtain a smaller size antenna element, but [14] requires a larger ground plane to obtain a relative bandwidth of 14%. The [13] has the problem of a higher profile and more complicated multilayer fabrication process. The proposed antenna in [20] uses a conventional symmetrical oscillator antenna using a ground plane as a reflector to obtain a gain of 3.4dBi. Finally, a comparison was made with the proposed antenna with the deletion of the deflector. The gain is significantly lower and the bandwidth is also reduced. Compared with the above antennas, the proposed end-fire array not only achieves end-fire performance but also has the advantage of small size $(0.43 \times 0.43 \times 0.02)\lambda_0$. Therefore, the proposed antenna can be widely used in devices requiring high gain and miniaturized antennas by using inverted F-loaded bending leads, and because of its low profile, the proposed antenna can be applied for easy integration with planar circuits, which is especially practical for millimeter-wave systems.

4. Conclusions

In summary, a novel inverted F-terminated array antenna with a low-profile feed structure suitable for millimeter-wave applications is proposed, and its structure, design process, and measurement results are given. The element consists of a horizontal printed inverted F antenna and a bent parasitic deflector, and the antenna array is fed by a SIW designed feed network. For demonstration purposes, a 1×4 array was fabricated and measured, showing a bandwidth of 20.5% (23–28.3 GHz) and a peak gain of 11 dB. Compared to other reported end-fire antennas, this element not only has a simple structure but also has the advantage of a low-profile feed structure and easy integration with planar circuits. It represents an ideal and promising candidate for broadband millimeter-wave applications.

Data Availability

The data that support the findings of this study are available from the corresponding author upon reasonable request.

Conflicts of Interest

The author(s) declare that there are no conflicts of interest regarding the publication of this paper.

References

[1] W. Hong, K.-H. Baek, Y. Lee, Y. Kim, and S. Ko, "Study and prototyping of practically large-scale mmWave antenna systems for 5G cellular devices," *IEEE Communications Magazine*, vol. 52, no. 9, pp. 63–69, Sep. 2014.

[2] L. Wei, R. Q. Hu, Y. Qian, and G. Wu, "Key elements to enable millimeter wave communications for 5G wireless systems," *IEEE Wireless Communications*, vol. 21, no. 6, pp. 136–143, Dec. 2014.

[3] J. Hasch, E. Topak, R. Schnabel, T. Zwick, R. Weigel, and C. Waldschmidt, "Millimeter-wave technology for

automotive radar sensors in the 77 GHz frequency band," *IEEE Transactions on Microwave Theory and Techniques*, vol. 60, no. 3, pp. 845–860, Mar. 2012.

[4] Y. Yu, W. Hong, and H. Zhang, "Optimization and implementation of SIW slot array for both medium- and long-range 77 GHz automotive radar application," *IEEE Transactions on Antennas and Propagation*, vol. 66, no. 7, pp. 3769–3774, Jul. 2018.

[5] Y. Rahmat-Samii and A. C. Densmore, "Technology trends and challenges of antennas for satellite communication systems," *IEEE Transactions on Antennas and Propagation*, vol. 63, no. 4, pp. 1191–1204, Apr. 2015.

[6] J. Wu, Y. J. Cheng, and Y. Fan, "A wideband high-gain high-efficiency hybrid integrated plate array antenna for V-band inter-satellite links," *IEEE Transactions on Antennas and Propagation*, vol. 63, no. 4, pp. 1225–1233, Apr. 2015.

[7] Y. Yu, Z. H. Jiang, H. Zhang, Z. Zhang, and W. Hong, "A low-profile beamforming patch array with a cosecant fourth power pattern for millimeter-wave synthetic aperture radar applications," *IEEE Transactions on Antennas and Propagation*, vol. 68, no. 9, pp. 6486–6496, 2020.

[8] Eddocs, *Allocation and Service Rules for the 71–76 GHz, 81–86 GHz, and 92–95 GHz Bands, Document FCC 03-248*, Federal communication Commission, 2003.

[9] Y. Yu, W. Hong, and Z. H. Jiang, "E-band low-profile, wideband 45° linearly polarized slot-loaded patch and its array for millimeter-wave communications," *IEEE Transactions on Antennas and Propagation*, vol. 66, no. 8, pp. 4364–4369, Aug. 2018.

[10] S. Verma, L. Mahajan, R. Kumar, H. S. Saini, and N. Kumar, *A Small Microstrip Patch Antenna for Future 5G Applications,* in *Proceedings of the 2016 5th International Conference on Reliability, Infocom Technologies and Optimization (Trends and Future Directions) (ICRITO)*, pp. 460–463, Noida, India, 07-09 September 2016.

[11] W. El-Halwagy, J. Mezler, M. Hossain, and P. Mousavi, "A 28 GHz compact vertically-polarized dipole for 5G smartphone edge," in *Proceedings of the 2017 IEEE International Symposium on Antennas and Propagation & USNC/URSI National Radio Science Meeting*, pp. 2573-2574, 09-14 July 2017.

[12] A. Zhao and F. Ai, "Dual-band 5G millimeter-wave MIMO antenna array for mobile phone application," in *Proceedings of the 12th European Conference on Antennas and Propagation (EuCAP 2018)*, London, UK, 09-13 April 2018.

[13] I. J. Hwang, B. K. Ahn, S. C. Chae, J. W. Yu, and W. W. Lee, "Quasi-yagi antenna array with modified folded dipole driver for mmWave 5G cellular devices," *IEEE Antennas and Wireless Propagation Letters*, vol. 18, no. 5, pp. 971–975, 2019.

[14] G. Hua, Y. Chen, and P. Lu, "Microstrip folded dipole antenna for 35 GHz MMW communication," *International Journal of Antennas and Propagation*, vol. 2013, pp. 1–6, 2013.

[15] W. Hong, S.-T. Ko, and Y. Lee, "Compact 28 GHz antenna array with full polarization flexibility under yaw, pitch, roll motions," in *Proceedings of the 9th Eur. Conf. Antennas Propag*, pp. 1–3, Lisbon, 13-17 April 2015.

[16] Y. W. Hsu, T. C. Huang, and H. S. Lin, "Dual-polarized quasi Yagi–Uda antennas with endfire radiation for millimeter-wave MIMO terminals," *IEEE Transactions on Antennas and Propagation*, vol. 65, no. 12, pp. 6282–6289, Dec. 2017.

[17] R. A. Alhalabi and G. M. Rebeiz, "High-efficiency angled-dipole antennas for millimeter-wave phased array applications," *IEEE Transactions on Antennas and Propagation*, vol. 56, no. 10, pp. 3136–3142, Oct. 2008.

[18] S. X. Ta, H. Choo, and I. Park, "Broadband printed-dipole antenna and its arrays for 5G applications," *IEEE Antennas and Wireless Propagation Letters*, vol. 16, pp. 2183–2186, 2017.

[19] J. Helander, K. Zhao, and Z. Ying, "Performance analysis of millimeter wave phased array antennas in cellular handsets," *IEEE Antennas and Wireless Propagation Letters*, vol. 15, pp. 504–507, 2016.

[20] H. Li, Y. Li, L. Chang, W. Sun, and X. Qin, "A wideband dual-polarized endfire antenna array with overlapped apertures and small clearance for 5G millimeter-wave applications," *IEEE Transactions on Antennas and Propagation*, no. 99, p. 1, 2020.

[21] Y. Liu, H. Lu, Y. Wu et al., "Millimeterwave and terahertz waveguide-fed circularly polarized antipodal curvedly tapered slot antennas," *IEEE Transactions on Antennas and Propagation*, vol. 64, no. 5, pp. 1607–1614, May 2016.

[22] Y. Yao, X. Cheng, and J. Yu, "Analysis and design of a novel circularly polarized antipodal linearly tapered slot antenna," *IEEE Transactions on Antennas and Propagation*, vol. 64, no. 10, pp. 4178–4187, Oct. 2016.

[23] Y. Yu, Z. H. Jiang, J.-D. Zhang, and W. Wu, "Broadband millimeter-wave endfire circularly polarized array with a low-profile feeding structure," *IEEE Transactions on Antennas and Propagation*, p. 1, 2022.

[24] A. Kumar, D. Chaturvedi, and S. I. Rosaline, "Design of antenna-multiplexer for seamless on-body internet of medical things (IoMT) connectivity," *IEEE Transactions on Circuits and Systems II: Express Briefs*, vol. 69, no. 8, pp. 3395–3399, 2019.

[25] F. Majid, M. Naser-Moghadasi, and R. Ali-Sadeghzadeh, "A broad band circularly polarized cross slot cavity back array antenna with sequentially rotated feed network for improving gain in X-band application," *International Journal of Microwave and Wireless Technologies*, vol. 1, no. 3, pp. 1–6, 2016.

[26] A. Kumar and S. Raghavan, "Broadband dual-circularly polarised SIW cavity antenna using a stacked structure," *Electronics Letters*, vol. 53, no. 17, pp. 1171-1172, 2017.

[27] K. Arvind, C. Divya, and R. Singaravelu, "SIW cavity-backed circularly polarized square ring slot antenna with wide axial-ratio bandwidth," *AEU - International Journal of Electronics and Communications*, vol. 94, p. S1434841118307520, 2018.